Mineralogical Magazine, August 2016, Vol. 80(5), pp. 719–732

H-bonding scheme in allactite: a combined single-crystal X-ray and neutron diffraction, optical absorption spectroscopy, FTIR and EPMA-WDS study

G. Diego Gatta[1,2,*], Ferdinando Bosi[3,4], Maria Teresa Fernandez Diaz[5] and Ulf Hålenius[6]

[1] Dipartimento di Scienze della Terra, Università degli Studi di Milano, Via Botticelli 23, I-20133 Milano, Italy
[2] CNR – Istituto di Cristallografia, Sede di Bari, Via G. Amendola 122/o, I-70126 Bari, Italy
[3] Dipartimento di Scienze della Terra, Sapienza Università di Roma, Piazzale Aldo Moro 5, I-00185 Roma, Italy
[4] CNR – Istituto di Geoscienze e Georisorse, UOS Roma, P.le Aldo Moro 5, 00185 Roma, Italy
[5] Institut Laue-Langevin, BP 156, F-38042 Grenoble Cedex 9, France
[6] Department of Geosciences, Swedish Museum of Natural History, Box 50007, SE-10405 Stockholm, Sweden

[*Received 19 May 2015; Accepted 12 July 2015; Associate Editor: Juraj Majzlan*]

ABSTRACT

The crystal chemistry of allactite from Långban, Värmland (Sweden) was investigated by single-crystal X-ray and neutron diffraction, optical absorption spectroscopy, Fourier-transform infra-red spectroscopy (FTIR) and electron microprobe analysis by wavelength-dispersive spectroscopy (EPMA-WDS). The optical spectra indicate the presence of Mn in valence state 2+ only. Assuming 16 O atoms per formula unit, arsenic as As^{5+} and the (OH) content calculated by charge balance, the resulting formula based on the EPMA-WDS data is $(Mn^{2+}_{6.73}Ca_{0.13}Mg_{0.12}Zn_{0.02})_{\Sigma 7.00}(As^{5+})_{2.00}O_{16}H_8$, very close to the ideal composition $Mn_7(AsO_4)_2(OH)_8$. In the unpolarized FTIR spectrum of allactite, fundamental (OH)-stretching bands are observed at 3236, 3288, 3387, 3446, 3484, 3562 and 3570 cm^{-1}, suggesting that a number of OH environments, with different hydrogen bond strengths, occur in the structure. The neutron structure refinement shows that four independent H sites occur in allactite with full site occupancy, all as members of hydroxyl groups. The complex hydrogen-bonding scheme in the allactite structure is now well defined, with at least nine hydrogen bonds energetically favourable with mono-, bi- and trifurcated configurations.

Keywords: allactite, arsenates, electron microprobe analysis, X-ray and neutron diffraction, optical absorption, infrared spectroscopy, hydrogen bonding.

Introduction

Allactite, ideally $Mn_7(AsO_4)_2(OH)_8$, is a member of the series of basic arsenates of manganese with general formula $Mn^{2+}_n(AsO_4)^{3-}_z(OH)^{-}_{2n-3z}$. This group of minerals occurs in low-temperature hydrothermal vein systems, associated with manganese-iron oxide ore bodies of the pyrometasomatic type in dolomitic marbles. There are only a few studies devoted to the mineralogy and crystal chemistry of allactite (Sjögren, 1884*a*,*b*; Moore, 1968; Welin, 1968; Dunn 1983; Frost and Weier, 2006), possibly due to the rarity of the mineral. Only a few occurrences are known worldwide: in veinlets through metamorphosed manganese deposits of the Moss and Brattfors mines, Nordmark (Sveden) and at Långban, Värmland (Sweden); in a metamorphosed stratiform zinc orebody at Franklin, Ogdensburg, Sussex Co., New Jersey (USA).

The crystal structure of allactite (from the type locality, Långban, Sweden) was solved and refined to a crystallographic *R* factor of 0.077 by Moore (1968), on the basis of X-ray intensity data collected with a Weissenberg apparatus. The allactite structure was found to be monoclinic, space group $P2_1/a$, unit-cell parameters $a = 11.03(2)$, $b = 12.12(2)$, $c = 5.51(1)$ Å, $\beta = 114.07°$ ($Z = 2$),

*E-mail: diego.gatta@unimi.it
DOI: 10.1180/minmag.2016.080.020

and a standard error on the refined bond distances of about 0.03. No further diffraction studies have so far been devoted to this mineral. The structure is built up of bands of octahedra, two octahedra wide, held together by vertex-linked octahedra, forming flat sheets (parallel to (001) in Fig. 1). These sheets are, in turn, held together by chains of linked Mn octahedra and As tetrahedra running parallel to [010] (Fig. 1). The bridging Mn octahedra connect to the sheets in a complicated fashion, exhibiting corner, edge and face sharing with them (Fig. 1). Based on the data of Moore (1968), the four independent Mn octahedra and the unique As tetrahedron appear to be significantly distorted. Despite that the structure model reported by Moore (1968) appears to be consistent, all the atom sites were modelled isotropically and no H site was located, making the H-bonding scheme unknown. Based on bond-valence arguments, Moore (1968) identified four O atoms belonging to the OH groups expected in the allactite structure. Later, the crystal structure of raadeite, ideally $Mg_7(PO_4)_2(OH)_8$, was published by Chopin *et al.* (2001). They described the structure of raadeite in the space group $P2_1/n$ with $a = 5.250(1)$, $b = 11.647(2)$, $c = 9.655(2)$ Å, $\beta = 95.94(1)°$ ($Z = 2$), recognizing the isostructural relation between raadeite and allactite and pointing out that Moore (1968) presented the allactite structure for a non-reduced cell. The reduced cell for allactite can be obtained from Moore's cell choice by the transformation [001/010/$\bar{1}0\bar{1}$]. Consistently, the structure of argandite, ideally $Mn_7(VO_4)_2(OH)_8$ (the V analogue of allactite) was later reported by Brugger *et al.* (2011) in the space group $P2_1/n$ with $a = 5.5038(2)$, $b = 12.2665(5)$, $c = 10.1055(5)$ Å, $\beta = 95.559(4)°$ ($Z = 2$), and the isostructural relation with allactite and raadeite was revealed. In the structure refinements of raadeite and argandite, four independent H sites were located by inspection of a difference-Fourier map. Proton sites were modelled isotropically and their positions were fixed (and not refined) in the raadeite refinement and refined in the argandite refinement. Raman and infrared spectra of allactite from Nordmark (Sweden) were reported by Frost and Weier (2006). Their infrared (ATR-IR) spectrum showed a very broad spectroscopic profile and, in addition, recorded strong OH-stretching bands at very high wave numbers (~3650 and ~3675 cm^{-1}). Frost and Weier (2006) assumed the distorted spectrum profile to be due to adsorbed water. They suggested that the reason for multiple bands in the OH-stretching region was caused by all 'OH units' not being at the same position in the structure, but offered no additional suggestions regarding hydrogen bonding in the mineral.

In order to obtain more precise structural and crystal chemical information, we have reinvestigated the crystal structure of allactite from the same locality as that studied previously by Moore (1968) by single-crystal X-ray and neutron diffraction, optical absorption spectroscopy, FTIR and EPMA-WDS. The aim of this study was to provide: (1) a crystal chemical characterization of this mineral, according to modern standards; (2) an unambiguous location of all the proton sites and the description of the complex H-bond network expected for the allactite structure, along with its low-*T* induced rearrangement; (3) the anisotropic displacement parameters of all the atom sites, including the H sites; and (4) the IR OH-stretching bands and their correlation with the H-bond scheme deduced on the basis of the neutron structure refinement.

As X-ray diffraction data did not accurately locate the H atoms in the allactite structure (Moore, 1968), single-crystal neutron diffraction represents the best experimental technique to answer the open questions about the crystal structure/crystal chemistry of this hydrous Mn-arsenate. The high crystalline quality, the chemical homogeneity, and the size of the allactite crystals from Långban make the mineral from this locality an excellent sample for a single-crystal neutron diffraction study.

Sample description and mineralogy

The present allactite specimen (NRM #19140395), from the collections of the Swedish Natural History Museum in Stockholm, was collected at the beginning of the 20th century at the well-known Långban Mn-Fe oxide deposit in central Sweden (Holtstam and Langhof, 1999). The specimen represents a ~15 cm thick, allactite-rich, late-stage vein that cuts dolomite-hosted oxide ore. The purplish-red coloured allactite single crystals attain sizes of up to 15 mm and they frequently show tabular forms on {100}. Allactite coexists with native lead, calcite, dolomite, domeykite and pyrochroite.

Experimental

Electron microprobe analysis

After X-ray investigation (see below), the same crystal of allactite was mounted on a glass slide, polished and carbon coated for EPMA-WDS analysis with a Cameca SX50 instrument at the Istituto di Geologia Ambientale e Geoingegneria (Rome, Italy), CNR, operating at 15 kV and 15 nA,

https://doi.org/10.1180/minmag.2016.080.020 Published online by Cambridge University Press

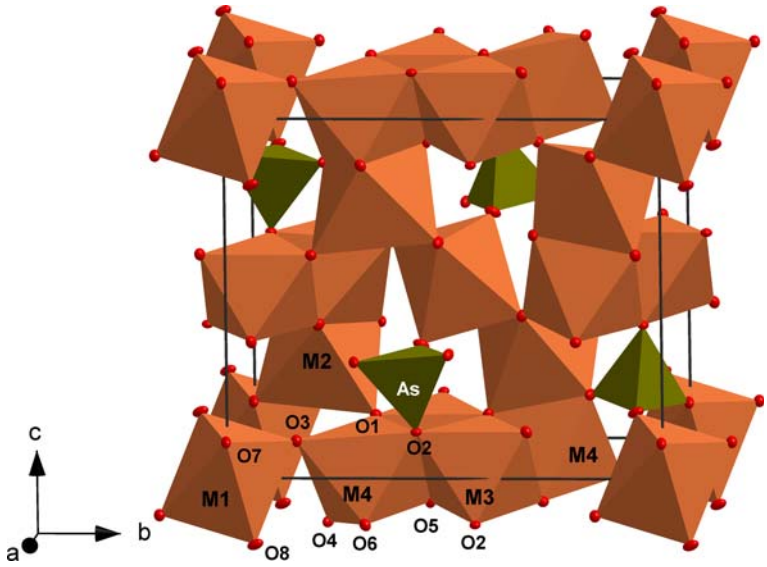

FIG. 1. Clinographic view of the crystal structure of allactite (H-free structure model), using the reduced cell with $a \approx 5.5$, $b \approx 12.1$, $c \approx 10.1$ Å and $\beta \approx 95.7°$, space group $P2_1/n$. The reduced cell can be obtained from the non-reduced cell choice of Moore (1968) with $a \approx 11.0$, $b \approx 12.1$, $c \approx 5.5$ Å and $\beta \approx 114.1°$, space group $P2_1/a$, by the transformation [001/010/$\bar{1}$01$\bar{1}$].

1 μm beam diameter. The following standards were used: wollastonite (Ca), olivine (Mg), rhodonite (Mn), sphalerite (Zn) and synthetic gallium arsenide (As). Wavelength-dispersive scans revealed no detectable amounts of any additional elements. The *PAP* routine was applied (Pouchou and Pichoir, 1991). Results are listed in Table 1.

Single-crystal X-ray diffraction

A representative fragment of the sample of allactite studied was selected for X-ray diffraction measurements on a Bruker KAPPA APEX-II single-crystal diffractometer, at the Sapienza University of Rome (Earth Sciences Department), equipped with a CCD area detector (6.2 cm × 6.2 cm active detection area, 512 × 512 pixels) and a graphite crystal monochromator, using Mo$K\alpha$ radiation from a fine-focus sealed X-ray tube. The sample-to-detector distance was set to 4 cm. A total of 4708 exposures (step = 0.2°, time/step = 20 s), covering a full reciprocal sphere with redundancy 4, was used (Table 2). Final unit-cell parameters were refined using the Bruker AXS *SAINT* program for reflections with $I > 10\sigma(I)$ in the range $2.5° < \theta < 40°$ (Bruker, 2008; Table 2). Intensity data were processed and corrected for Lorentz, polarization, and background effects with the *APEX2* software program of Bruker AXS (Bruker, 2008). Data were corrected for absorption using the multi-scan method (*SADABS*; Bruker, 2008). The absorption correction led to a significant improvement in R_{int}. The diffraction pattern was indexed with the reduced unit cell reported in Table 2. Reflection conditions suggested the $P2_1/n$ space group.

TABLE 1. Chemical composition of allactite based on EPMA-WDS.

	wt.%		apfu
As_2O_5	28.8(4)	As^{5+}	2.00
MnO	59.8(5)	Mn^{2+}	6.73
MgO	0.61(3)	Mg	0.12
ZnO	0.17(7)	Zn	0.02
CaO	0.88(3)	Ca	0.13
H_2O[a]	9.03	OH	8.00
Total	99.34		

Number of atoms calculated on the basis of 16 oxygen atoms; estimated standard deviations in brackets; apfu = atoms per formula unit. [a]Calculated by stoichiometry.

Single-crystal neutron diffraction

A prismatic crystal of allactite (3.8 mm × 3.2 mm × 2.8 mm), free of defects under the polarized optical microscope, was selected for the neutron diffraction

https://doi.org/10.1180/minmag.2016.080.020 Published online by Cambridge University Press

TABLE 2. Details of X-ray and neutron data collections and refinements of allactite.

T (K)	293	293	100
Crystal shape	Prismatic	Prismatic	Prismatic
Crystal size (mm)	0.28 × 0.26 × 0.25	3.8 × 3.2 × 2.8	3.8 × 3.2 × 2.8
Crystal colour	Purplish red	Purplish red	Purplish red
Unit cell constants (Å, °)	a = 5.5225(1)	a = 5.482(1)	a = 5.4786(8)
	b = 12.2760(3)	b = 12.153(2)	b = 12.156(2)
	c = 10.1230(2)	c = 10.014(2)	c = 10.008(1)
	β = 95.632(1)	β = 95.55(1)	β = 95.574(8)
Reference formula	$Mn_7(AsO_4)_2(OH)_8$	$Mn_7(AsO_4)_2(OH)_8$	$Mn_7(AsO_4)_2(OH)_8$
Space group	$P2_1/n$	$P2_1/n$	$P2_1/n$
Z	2	2	2
Radiation	Monochromatic, X-ray	Monochromatic, neutron	Monochromatic, neutron
Diffractometer	Bruker KAPPA APEX-II	D9 ILL	D9 ILL
λ (Å)	Mo$K\alpha$	0.8370	0.8370
θ_{max}(Å)	40.0	34.6	32.6
	$-9 \le h \le 8$	$-7 \le h \le 2$	$-6 \le h \le 2$
	$-21 \le k \le 21$	$-13 \le k \le 16$	$-12 \le k \le 15$
	$-18 \le l \le 18$	$-12 \le l \le 13$	$-11 \le l \le 12$
No. measured reflections	17,817	2222	2063
No. unique reflections	3916	1561	1278
No. unique refl. with $F_o > 4\sigma(F_o)$	3632	1362	1160
No. refined parameters	131	152	152
R_{int}	0.0205	0.0403	0.0255
R_1 (F) with $F_o > 4\sigma(F_o)$	0.0173	0.0421	0.0331
R_1 (F) for all the unique reflections	0.0195	0.0501	0.0388
wR_2 (F^2)	0.0423	0.0858	0.0622
Residuals (e Å^{-3}, fm Å^{-3})	–0.55/+0.60	–0.66/+0.82	–0.42/+0.46

$R_{int} = \Sigma \mid F^2_{obs} - F^2_{obs}(mean) \mid / \Sigma [F^2_{obs}]$; $R_1 = \Sigma||F_{obs}| - |F_{calc}||/\Sigma|F_{obs}|$; $wR_2 = [\Sigma[w(F^2_{obs} - F^2_{calc})^2]/\Sigma[w(F^2_{obs})^2]]^{0.5}$, $w = 1/[\sigma^2(F^2_{obs}) + (aP)^2 + bP]$, $P = (\text{Max } (F^2_{obs}, 0) + 2F^2_{calc})/3$. Refined extinction coefficient (as implemented in *Shelx*): 0.0080(3) for X-ray data, 0.061(2) for neutron data at 293 K.

experiments. Neutron diffraction data were measured at 293 and 100 K on the four-circle diffractometer D9, at the high-flux research reactor of the Institut Laue-Langevin (ILL) in Grenoble, France, with a neutron beam of wavelength 0.8370(2) Å, obtained by reflection from a Cu(220) monochromator. The D9 diffractometer is equipped with a small two-dimensional area detector (Lehmann *et al.*, 1989), which allowed optimum resolution of the peaks from background. Diffraction data were collected to θ_{max} 34.6 and 32.6° at 293 and 100 K, respectively (*h, k, l* ranges are listed in Table 2). For all data, background corrections following Wilkinson *et al.* (1988) and Lorentz corrections were applied. Absorption corrections were made by Gaussian integration (Coppens *et al.*, 1965), using the calculated attenuation coefficient with an account taken of the wavelength dependence of the absorption for the hydrogen content (Howard *et al.*, 1987). Initial structural refinements showed that extinction affected only a few reflections, and could be well accounted for by the simple isotropic extinction model in *SHELX-97* (Sheldrick, 2008). The low degree of extinction meant that the data could be averaged over symmetry-equivalent reflections. Averaging in the 2/*m* Laue class of the 2222 (at 293 K) and 2063 (at 100 K) reflections scanned gave 1561 (at 293 K) and 1278 (at 100 K) unique reflections with an internal discrepancy index of 0.0403 (at 293 K) and 0.0255 (at 100 K). As the three-dimensional count distribution around each reflection was observed, the centroids of all scanned reflections could be found. Least-squares matching of the observed and calculated centroids of a few hundreds of the strongest reflections for the collections at 293 K and at 100 K gave the unit-cell parameters listed in Table 2. The reflection conditions suggested space group $P2_1/n$. Other details pertaining to the neutron data collections are listed in Table 2.

https://doi.org/10.1180/minmag.2016.080.020 Published online by Cambridge University Press

Optical absorption and Fourier-transform infra-red spectroscopy

Polarized optical absorption spectra at 293 K were recorded in the range 270–1700 nm (37,037–5882 cm^{-1}) on two 88 μm thick, doubly-sided polished platelets prepared from a single crystal of allactite. The two platelets represented the optical *XY* and *YZ* planes, respectively. The orientations of the platelets were confirmed by optical microscopy using conoscopic imaging. Spectra were recorded at a resolution of 1 nm using an AvaSpec-ULS2048X16 spectrometer (270–1060 nm) attached via a 400 μm UV optical fibre to a Zeiss Axiotron UV microscope, and at a resolution of 3 nm using an AvaSpec-NIR256-1.7TEC spectrometer (1060–1700 nm) attached via a 400 μm IR optical fibre to the same microscope. A 75 W Xenon arc lamp (270–1060 nm) and a 100 W halogen lamp (1060–1700 nm) served as illuminating sources and Zeiss Ultrafluar 10x lenses served as objective and condenser. A UV quality Glan-Thompson prism with a working range from 250 to 2700 nm (40,000 to 3704 cm^{-1}) was used as polarizer. The size of the circular measuring aperture was 200 μm. The wavelength scale of the spectrometer was calibrated against Ho_2O_3-doped and Pr_2O_3/Nd_2O_3-doped standards (Hellma glass filters 666F1 and 666F7) with an accuracy better than 15 cm^{-1} in the wavelength range 300–1100 nm. A pressed KBr disc mixed with ~1 mg of powdered allactite sample was measured by FTIR to characterize OH absorption bands in the 2000–5000 cm^{-1} range using a Bruker Equinox 55 spectrometer equipped with a NIR source, a CaF_2 beam-splitter and an InSb detector. The unpolarized FTIR-spectrum was acquired during 256 cycles at a nominal resolution of 4 cm^{-1}. Collected spectra were fitted using Jandel *PeakFit* 4.12 software, assuming Gaussian peak shapes.

Results

X-ray and neutron structure refinements

Anisotropic crystal structure refinements based on the X-ray and neutron intensity data were performed using *SHELXL* software (Sheldrick, 2008), starting from the structure model of Moore (1968), but using the reduced-cell choice reported by Chopin *et al.* (2001) for raadeite (Table 2). Variable parameters for the X-ray refinement were scale factor, isotropic extinction parameter, atom coordinates, atom displacement factors, and site-scattering values expressed as site occupancy factor (s.o.f.) for the *M*1, *M*3 and *M*4 sites (Table 3*a*). Refinement was conducted using neutral scattering factors (Wilson and Prince, 1999), and modelling the octahedrally coordinated sites *M*1, *M*2, *M*3 and *M*4 with Mn, the tetrahedrally coordinated site with As, and the anion sites with O. The *M*2, *As* and anion sites were modelled with a fixed occupancy of 1, because refinement with unconstrained occupancies showed no significant deviations from this value. Four independent H sites were located by inspection of the maxima in difference-Fourier maps; their positions were then refined, but fixing the displacement parameters (Table 3*a*). With this structure model, convergence was achieved rapidly and the variance-covariance matrix showed no significant correlations between the refined parameters. Further details pertaining to the structure refinements are given in Table 2; fractional atomic coordinates, site occupancy and displacement parameters are listed in Table 3*a*; Table 4 shows selected bond distances. The calculated density is 3.856 g cm^{-3}.

Neutron refinements (at 293 and 100 K) were conducted with the neutron scattering lengths of Mn, As, O and H according to Sears (1986). Correction for secondary isotropic extinction was performed according to the protocol of Larson (1967). Refinements were conducted with the scattering length of manganese at the *M*1, *M*2, *M*3 and *M*4 sites, the length of arsenic at the *As* site and that of oxygen at the eight independent O sites (i.e. *O*1–8) (Tables 3*b*,*c*). The first cycles of refinements were conducted without any H sites. When convergence was achieved, the difference-Fourier maps of the nuclear density showed four independent negative residuals, at ~1 Å from the *O*1, *O*3, *O*5 and *O*6 sites. The structure model was then implemented with four additional sites occupied by hydrogen (here labelled as *H*1, *H*3, *H*5 and *H*6; Tables 3*b*,*c*), as hydrogen has a negative neutron scattering length [(b_c(H) = –3.7409 fm; Sears, 1986]. All sites showed no significant deviation from full occupancy. With such a structure model, convergence was achieved rapidly and the variance-covariance matrix showed no significant correlation among the refined parameters. At the end of the last cycles of the refinement, no peaks larger than ±0.8 fm $Å^{-3}$ were present in the final difference-Fourier map of nuclear density (Table 2). The final R_1 was 0.0421 (at 293 K) and 0.0331 (at 100 K) for 152 refined parameters and 1362 (at 293 K) and 1160 (at 100 K) unique reflections with $F_o > 4\sigma(F_o)$

https://doi.org/10.1180/minmag.2016.080.020 Published online by Cambridge University Press

TABLE 3a. Atom coordinates and displacement parameters (Å^2) for the expression $2\pi^2[(ha^*)^2U^{11} + \ldots + 2hka^*b^*U^{12} + \ldots + 2klb^*c^*U^{23}]$, based on the X-ray structure refinement at 293 K. U_{eq} is defined as one third of the trace of the orthogonalized U^{ij} tensor. The site-occupancy factor is 1 for As, O and H sites.

Site	*x*/*a*	*y*/*b*	*z*/*c*	$U_{eq/iso}$	U^{11}	U^{22}	U^{33}	U^{23}	U^{13}	U^{12}
*M*1	0	0	0	0.01198(6)	0.01383(12)	0.01089(9)	0.01118(9)	–0.00069(6)	0.00101(7)	–0.00116(7)
*M*2	0.26943(3)	0.18010(2)	0.20916(2)	0.01325(4)	0.01298(8)	0.01242(6)	0.01383(7)	–0.00170(5)	–0.00137(5)	0.00114(5)
*M*3	0.25119(3)	0.43095(2)	0.99254(2)	0.01153(5)	0.00931(9)	0.01120(7)	0.01390(7)	–0.00007(5)	0.00028(5)	–0.00052(4)
*M*4	0.24882(3)	0.21051(2)	0.50019(2)	0.01188(5)	0.01160(9)	0.01186(7)	0.01219(7)	0.00092(5)	0.00129(5)	–0.00035(5)
As	0.03424(2)	0.57922(2)	0.70814(2)	0.00843(3)	0.00802(5)	0.00823(4)	0.00895(4)	–0.00013(3)	0.00034(3)	0.00000(3)
*O*1	0.44857(16)	0.30618(6)	0.11469(8)	0.01301(13)	0.0129(4)	0.0133(3)	0.0128(3)	0.0006(2)	0.0014(2)	–0.0001(2)
*O*2	0.05926(15)	0.57025(6)	0.87826(8)	0.01133(12)	0.0116(3)	0.0128(3)	0.0094(3)	0.0006(2)	0.0001(2)	0.0003(2)
*O*3	0.07435(16)	0.84594(7)	0.90412(8)	0.01427(13)	0.0130(4)	0.0139(3)	0.0157(3)	0.0012(2)	0.0007(3)	0.0011(2)
*O*4	0.91527(17)	0.70196(6)	0.66775(8)	0.01638(15)	0.0232(4)	0.0112(3)	0.0143(3)	0.0018(2)	–0.0002(3)	0.0059(3)
*O*5	0.07742(16)	0.06280(6)	0.38765(8)	0.01345(13)	0.0124(4)	0.0118(3)	0.0160(3)	–0.0006(2)	0.0006(3)	–0.0003(2)
*O*6	0.54268(16)	0.18377(6)	0.37529(8)	0.01337(13)	0.0112(3)	0.0130(3)	0.0155(3)	0.0029(2)	–0.0007(3)	–0.0012(2)
*O*7	0.85266(16)	0.47996(7)	0.63903(8)	0.01462(14)	0.0157(4)	0.0126(3)	0.0147(3)	0.0004(2)	–0.0027(3)	–0.0050(2)
*O*8	0.32017(16)	0.57296(7)	0.66451(9)	0.01628(15)	0.0096(4)	0.0236(4)	0.0160(3)	–0.0046(3)	0.0030(3)	–0.0007(3)
*H*1	0.512(3)	0.3450(14)	0.1886(15)	0.016						
*H*3	0.179(3)	0.8674(15)	0.8498(16)	0.017						
*H*5	0.029(3)	0.0252(14)	0.3160(15)	0.016						
*H*6	0.626(3)	0.2478(12)	0.3673(17)	0.016						

s.o.f.(*M*1) = 0.979(1); s.o.f.(*M*2) = 1; s.o.f.(*M*3) = 0.986(1); s.o.f.(*M*4) = 0.979(1); equivalent (U_{eq}) and isotropic (U_{iso}) displacement parameters; *H*1,3,5,6 sites were constrained to have a $U_{iso} = 1.2\ U_{eq}$ of the co-respective *O*1,3,5,6 sites.

TABLE 3b. Atom coordinates and displacement parameters (Å^2) for the expression $2\pi^2[(ha^*)^2U^{11} + \ldots + 2hka^*b^*U^{12} + \ldots + 2klb^*c^*U^{23}]$, based on the neutron structure refinement at 293 K. U_{eq} is defined as one third of the trace of the orthogonalized U^{ij} tensor. The site-occupancy factor is 1 for all the sites.

Site	*x*/*a*	*y*/*b*	*z*/*c*	U_{eq}	U^{11}	U^{22}	U^{33}	U^{23}	U^{13}	U^{12}
*M*1	0	0	0	0.0119(5)	0.0135(13)	0.0114(12)	0.0108(11)	–0.0004(9)	0.0016(10)	0.0001(9)
*M*2	0.2686(4)	0.1796(1)	0.2091(2)	0.0115(4)	0.0148(9)	0.0096(8)	0.0097(8)	–0.0023(6)	–0.0014(7)	0.0009(7)
*M*3	0.2516(4)	0.4306(2)	0.9923(3)	0.0160(4)	0.0170(10)	0.0155(9)	0.0154(9)	–0.0004(7)	0.0004(8)	–0.0001(9)
*M*4	0.2478(4)	0.2108(2)	0.5007(2)	0.0168(4)	0.0200(10)	0.0150(9)	0.0155(9)	0.0014(7)	0.0017(8)	–0.0006(8)
As	0.0340(2)	0.57939(8)	0.70777(9)	0.0068(2)	0.0085(5)	0.0053(4)	0.0064(4)	–0.0001(3)	–0.0002(4)	0.0001(4)
*O*1	0.4489(2)	0.3060(1)	0.1147(1)	0.0117(3)	0.0141(6)	0.0112(5)	0.0096(5)	–0.0001(4)	–0.0002(5)	–0.0005(5)
*O*2	0.0599(2)	0.5702(1)	0.8780(1)	0.0100(2)	0.0131(6)	0.0108(5)	0.0060(5)	0.0005(4)	0.0001(4)	0.0009(5)
*O*3	0.0756(2)	0.8466(1)	0.9048(1)	0.0118(3)	0.0124(6)	0.0107(5)	0.0117(5)	–0.0001(4)	–0.0014(5)	0.0015(5)
*O*4	0.9170(3)	0.7023(1)	0.6678(1)	0.0139(3)	0.0217(7)	0.0093(5)	0.0102(5)	0.0003(4)	–0.0009(5)	0.0046(5)
*O*5	0.5771(2)	0.4375(1)	0.8870(1)	0.0121(3)	0.0134(6)	0.0100(5)	0.0127(6)	0.0009(4)	0.0007(5)	0.0006(5)
*O*6	0.5425(2)	0.1838(1)	0.3751(1)	0.0118(3)	0.0118(6)	0.0115(6)	0.0119(5)	0.0022(4)	–0.0008(4)	–0.0014(5)
*O*7	0.8516(3)	0.4805(1)	0.6390(1)	0.0128(3)	0.0178(7)	0.0089(5)	0.0108(5)	0.0001(4)	–0.0034(5)	–0.0039(5)
*O*8	0.3203(2)	0.5726(1)	0.6640(1)	0.0147(3)	0.0118(6)	0.0215(6)	0.0111(5)	–0.0053(5)	0.0022(5)	–0.0018(5)
*H*1	0.5129(5)	0.3473(2)	0.1935(2)	0.0236(5)	0.0296(13)	0.0237(11)	0.0170(10)	–0.0047(9)	0.0001(9)	–0.0020(10)
*H*3	0.1805(6)	0.8674(2)	0.8399(3)	0.0350(6)	0.0347(15)	0.0384(15)	0.0342(14)	0.0130(12)	0.0153(12)	0.0026(12)
*H*5	0.5257(6)	0.4731(2)	0.8045(2)	0.0299(6)	0.0472(16)	0.0272(12)	0.0145(10)	0.0031(9)	–0.0017(10)	0.0011(11)
*H*6	0.6352(5)	0.2504(2)	0.3711(2)	0.0295(6)	0.0318(14)	0.0259(13)	0.0299(12)	0.0068(10)	–0.0017(10)	–0.0116(12)

TABLE 3c. Atom coordinates and displacement parameters (Å^2) for the expression $2\pi^2[(ha^*)^2U^{11} + \ldots + 2hka^*b^*U^{12} + \ldots + 2klb^*c^*U^{23}]$, based on the neutron structure refinement at 100 K. U_{eq} is defined as one third of the trace of the orthogonalized U^{ij} tensor. The site-occupancy factor is 1 for all the sites.

Site	*x*/*a*	*y*/*b*	*z*/*c*	U_{eq}	U^{11}	U^{22}	U^{33}	U^{23}	U^{13}	U^{12}
*M*1	0	0	0	0.0081(5)	0.0116(13)	0.0065(11)	0.0061(10)	0.0001(9)	0.0006(9)	–0.0007(9)
*M*2	0.2683(3)	0.1796(1)	0.2094(2)	0.0063(3)	0.0073(9)	0.0050(7)	0.0064(7)	–0.0012(6)	–0.0007(6)	–0.0003(7)
*M*3	0.2513(3)	0.4310(2)	0.9930(2)	0.0120(4)	0.0136(7)	0.0101(8)	0.0123(8)	0.0005(7)	0.0014(7)	–0.0007(8)
*M*4	0.2482(4)	0.2101(1)	0.5004(2)	0.0135(4)	0.0166(9)	0.0110(9)	0.0134(8)	0.0001(7)	0.0034(7)	–0.0001(8)
As	0.0354(2)	0.57926(7)	0.70789(9)	0.0048(2)	0.0055(5)	0.0036(4)	0.0053(4)	0.0001(3)	0.0003(3)	0.0009(4)
*O*1	0.4480(2)	0.30627(9)	0.1151(1)	0.0076(2)	0.0084(6)	0.0071(5)	0.0076(5)	0.0001(4)	0.0013(4)	–0.0006(5)
*O*2	0.0603(2)	0.56991(9)	0.8786(1)	0.0067(2)	0.0082(5)	0.0063(5)	0.0055(4)	0.0004(4)	0.0001(4)	0.0001(5)
*O*3	0.0767(2)	0.84634(9)	0.9048(1)	0.0075(2)	0.0077(6)	0.0062(5)	0.0083(5)	–0.0003(4)	0.0001(5)	0.0006(5)
*O*4	0.9183(2)	0.70253(9)	0.6679(1)	0.0079(2)	0.0107(6)	0.0055(5)	0.0075(5)	0.0004(4)	0.0004(4)	0.0024(5)
*O*5	0.5771(2)	0.43729(9)	0.8866(1)	0.0075(2)	0.0088(6)	0.0050(5)	0.0087(5)	0.0004(4)	0.0003(4)	0.0002(5)
*O*6	0.5431(2)	0.18381(9)	0.3751(1)	0.0073(2)	0.0084(6)	0.0047(5)	0.0087(5)	0.0010(4)	–0.0005(4)	–0.0014(5)
*O*7	0.8522(2)	0.48012(9)	0.6384(1)	0.0070(2)	0.0081(5)	0.0052(5)	0.0074(5)	0.0002(4)	–0.0010(4)	–0.0019(5)
*O*8	0.3227(2)	0.57240(9)	0.6645(1)	0.0080(2)	0.0064(5)	0.0104(5)	0.0075(5)	–0.0019(4)	0.0017(4)	0.0001(5)
*H*1	0.5136(4)	0.3476(2)	0.1942(2)	0.0200(5)	0.0238(12)	0.0191(10)	0.0164(10)	–0.0044(9)	–0.0014(9)	–0.0027(9)
*H*3	0.1840(4)	0.8667(2)	0.8398(2)	0.0246(5)	0.0226(12)	0.0278(11)	0.0252(11)	0.0061(9)	0.0116(10)	–0.0002(10)
*H*5	0.5239(4)	0.4733(2)	0.8036(2)	0.0234(5)	0.0330(13)	0.0244(11)	0.0122(10)	0.0040(10)	–0.0005(9)	0.0020(10)
*H*6	0.6345(4)	0.2512(2)	0.3715(2)	0.0240(5)	0.0282(13)	0.0156(11)	0.0277(11)	0.0043(8)	0.0005(9)	–0.0103(10)

TABLE 4. Relevant bond distances (Å) and angles (°) based on the X-ray (XR) and neutron (N) structure refinements for allactite at 293 K and 100 K.

T (K)	XR-293	N-293	N-100
*M*1–*O*3 × 2	2.1830(8)	2.152(1)	2.157(1)
*M*1–*O*8 × 2	2.2106(8)	2.182(1)	2.177(1)
*M*1–*O*7 × 2	2.3014(8)	2.278(1)	2.276(1)
<*M*1–*O*>	2.232	2.204	2.203
*M*2–*O*1	2.1152(8)	2.100(2)	2.100(2)
*M*2–*O*6	2.1469(8)	2.130(2)	2.129(2)
*M*2–*O*3	2.1435(9)	2.132(2)	2.136(2)
*M*2–*O*7	2.1541(8)	2.133(2)	2.134(2)
*M*2–*O*4	2.2223(8)	2.204(2)	2.202(2)
*M*2–*O*5	2.6151(9)	2.581(2)	2.574(2)
<*M*2–*O*>	2.233	2.213	2.212
*M*3–*O*6	2.1094(8)	2.089(2)	2.093(2)
*M*3–*O*5	2.1821(8)	2.166(2)	2.163(2)
*M*3–*O*5	2.1805(9)	2.160(3)	2.167(2)
*M*3–*O*1	2.1906(8)	2.171(2)	2.167(2)
*M*3–*O*2	2.2561(8)	2.243(2)	2.234(2)
*M*3–*O*2	2.2684(8)	2.249(2)	2.242(2)
<*M*3–*O*>	2.198	2.180	2.178
*M*4–*O*3	2.1143(8)	2.093(2)	2.095(2)
*M*4–*O*1	2.1242(8)	2.096(3)	2.104(2)
*M*4–*O*4	2.1362(8)	2.117(2)	2.122(2)
*M*4–*O*6	2.1777(9)	2.167(3)	2.163(2)
*M*4–*O*5	2.2955(8)	2.283(2)	2.276(2)
*M*4–*O*2	2.3121(8)	2.293(2)	2.285(2)
<*M*4–*O*>	2.193	2.175	2.174
As–*O*4	1.6783(8)	1.659(1)	1.664(1)
As–*O*7	1.6859(8)	1.669(2)	1.676(1)
As–*O*8	1.6826(9)	1.672(2)	1.675(1)
As–*O*2	1.7176(8)	1.701(1)	1.705(1)
<*As*–*O*>	1.691	1.675	1.680
*O*1–*H*	0.93(1)	0.972(2)	0.977(3)
*O*1–*H*1*		0.987	0.993
*O*1···*O*8		2.854(3)	2.842(2)
*H*1···*O*8		1.888(3)	1.871(3)
*O*1–*H*1···*O*8		172.0(2)	172.6(2)
*O*3–*H*3	0.88(1)	0.943(2)	0.951(2)
*O*3–*H*3*		0.978	0.976
*O*3···*O*5		3.160(3)	3.155(2)
*H*3···*O*5		2.695(3)	2.699(3)
*O*3–*H*3···*O*5		111.2(2)	110.1(2)
*O*3···*O*6		3.676(3)	3.668(1)
*H*3···*O*6		2.822(3)	2.804(2)
*O*3–*H*3···*O*6		151.2(2)	151.5(2)
*O*3···*O*7		3.601(3)	3.589(2)
*H*3···*O*7		2.900(3)	2.880(3)
*O*3–*H*3···*O*7		132.1(2)	132.3(2)
*O*5–*H*5	0.88(1)	0.951(2)	0.959(3)
*O*5–*H*5*		0.977	0.981
*O*5···*O*8		3.009(3)	2.996(2)
*H*5···*O*8		2.098(3)	2.075(3)
*O*5–*H*5···*O*8		159.9(2)	160.6(2)
*O*5···*O*7		3.071(3)	3.072(1)
*H*5···*O*7		2.553(3)	2.560(2)
*O*5–*H*5···*O*7		114.4(2)	113.6(2)
*O*5···*O*3		3.160(3)	3.155(2)
*H*5···*O*3		2.615(3)	2.610(2)
*O*5–*H*5···*O*3		116.8(2)	116.4(2)
*O*6–*H*6	0.92(1)	0.959(2)	0.963(3)
*O*6–*H*6*		0.983	0.986
*O*6···*O*8		3.089(3)	3.088(2)
*H*6···*O*8		2.197(3)	2.190(3)
*O*6–*H*6···*O*8		154.3(2)	154.6(2)
*O*6···*O*4		3.336(3)	3.324(2)
*H*6···*O*4		2.587(3)	2.581(3)
*O*6–*H*6···*O*4		135.1(2)	134.1(2)

(continued)

TABLE 4. (*contd*.)

*Bond distance corrected for 'riding motion' following Busing and Levy (1964).

(Table 2). Site coordinates and displacement parameters are given in Tables 3*b*,*c* and relevant bond lengths and angles in Table 4.

Optical and FTIR spectroscopy

Polarized optical absorption spectra (Fig. 2) show a set of sharp to moderately sharp electronic *d*-*d* bands typical of Mn^{2+} in oxygen-based minerals (Burns, 1993; Hålenius *et al.*, 2007). The molar absorption coefficients (ε) of the bands range up to 1.0 L mol^{-1} cm^{-1}, which suggests that they may be related to electronic transitions in Mn^{2+} cation pairs in edge- or face-sharing octahedra (Lohr and McClure, 1968). In view of the structure of allactite that consists of edge-sharing octahedra, this is not surprising. The energies of the absorption bands and their assignments are summarized in Table 5. Tentative band assignments are based on the present crystal-structure information for allactite and on the relationship between the energies of the $^6A_1(S) \rightarrow {}^4E_g(D)$ and $^6A_1(S) \rightarrow {}^4E_g\,{}^4A_{1g}(G)$ bands in octahedrally and tetrahedrally coordinated Mn^{2+} observed in a large set of minerals and inorganic substances (Hålenius *et al.*, 2007). The proposed assignments result in very reasonable Racah *B* and *C* parameters as well as crystal field-splitting parameters typical of octahedrally coordinated Mn^{2+}. A slightly higher 10*Dq* calculated for Mn^{2+} at the *M*2, *M*3 and *M*4 sites in relation to the value for Mn^{2+} at

https://doi.org/10.1180/minmag.2016.080.020 Published online by Cambridge University Press

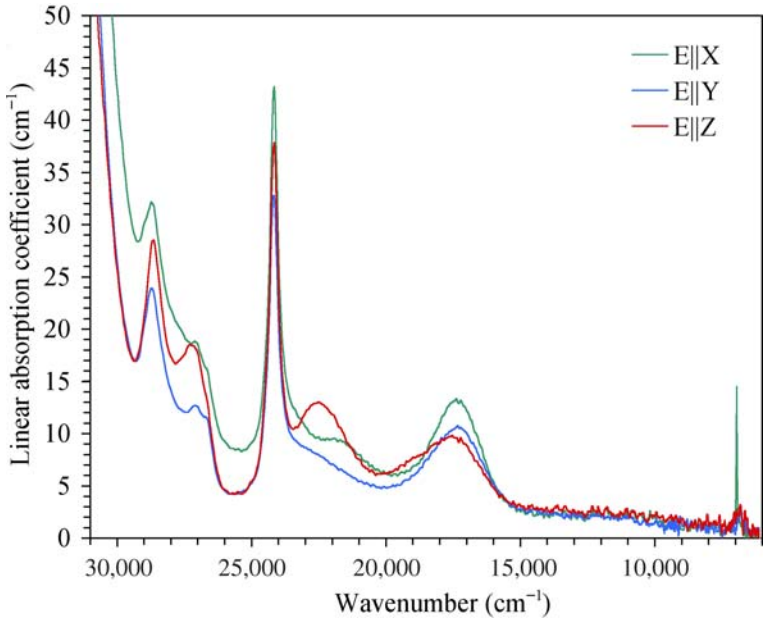

FIG. 2. Polarized optical absorption spectra of allactite.

the *M*1 site reflects that the *M*1 site is coordinated by 4 O^{2-} and 2 OH^{-}, while the remaining *M*2–4 sites are coordinated by 2 O^{2-} and 4 OH^{-} (Table 4). The present optical spectra show no indication of a presence of other Mn valence states than Mn^{2+}.

In addition to the spin-forbidden electronic Mn^{2+} *d-d* bands, overtones of OH-stretching modes are recorded in the NIR spectra at 6950 and 6965 cm^{-1}. In the unpolarized FTIR spectrum of allactite (Fig. 3), fundamental OH-stretching bands are observed at 3236, 3288, 3387, 3446, 3484, 3562 and 3570 cm^{-1}. In contrast to the infrared spectrum of allactite published by Frost and Weir (2006), our IR spectrum shows narrow and well-defined stretching bands and their recorded bands at ~3650 and ~3675 cm^{-1} are not reproduced. Our spectrum demonstrates that a number of OH environments, with different hydrogen-bond strengths, occur in the allactite structure. Based on observed relationships between O···H distances as determined by diffraction studies and OH-stretching band energies (Libowitzky, 1999), the observed OH bands in the spectrum of allactite suggest that O···H distances in the mineral range from ~1.81 to ~2.21 Å. Infrared spectra of the isostructural minerals raadeite $[Mg_7(PO_4)_2(OH)_8]$ and argandite $[Mg_7(PO_4)_2(OH)_8]$ show OH-stretching bands in comparable ranges (Chopin *et al.* 2001; Brugger *et al.*, 2011).

Discussion

EPMA-WDS data of the allactite sample from Långban confirm the previous experimental findings of Moore (1968). Atomic fractions were calculated assuming that the valence state of Mn is 2+, as indicated by optical spectroscopy, and the valence state of As is 5+ on the basis of the allactite stoichiometry (Table 1). Assuming 16 O atoms per formula unit (apfu) and the OH content calculated by charge balance, the resulting unit formula is $(Mn^{2+}_{6.73}Ca_{0.13}Mg_{0.12}Zn_{0.02})_{\Sigma 7.00}(As^{5+})_{2.00}O_{16}H_8$, very close to the end-member composition $Mn_7(AsO_4)_2(OH)_8$. X-ray and neutron structure refinements corroborate the crystal chemistry of allactite, and the site populations at the octahedrally coordinated sites *M*1, *M*2, *M*3 and *M*4, modelled following the protocol of Wright *et al.* (2000) and using the X-ray structural data, leads to the structural formula $^{M1}(Mn^{2+}_{0.85}Ca_{0.13}Zn_{0.02})_{\Sigma 1.00}{}^{M2}(Mn^{2+}_{2.00})$ $^{M3}(Mn^{2+}_{1.95}Mg_{0.05})_{\Sigma 2.00}{}^{M4}(Mn^{2+}_{1.92}Mg_{0.08})_{\Sigma 2.00}(AsO_4)_2$ $(OH)_8$. There is an excellent match between the number of electrons per formula unit (epfu) on the basis of the EPMA-WDS data and those obtained by the X-ray structure refinement, 238.8 and 238.7 epfu, respectively. There is a slight difference in the lengths of unit-cell edges obtained by X-ray and

https://doi.org/10.1180/minmag.2016.080.020 Published online by Cambridge University Press

TABLE 5. Positions and assignments of *d-d* bands and crystal field parameters for $^{VI}Mn^{2+}$ in allactite (see text for details).

ν (cm^{-1})	*M*1	*M*2, *M*3, *M*4
29,020		$^6A_1(S) \rightarrow {}^4E_g(D)$
28,675	$^6A_1(S) \rightarrow {}^4E_g(D)$	
27,140	$^6A_1(S) \rightarrow {}^4T_{2g}(D)$	
26,690		$^6A_1(S) \rightarrow {}^4T_{2g}(D)$
24,470		$^6A_1(S) \rightarrow {}^4E_g{}^4A_{1g}(G)$
24,180	$^6A_1(S) \rightarrow {}^4E_g{}^4A_{1g}(G)$	
22,520	$^6A_1(S) \rightarrow {}^4T_{2g}(G)$	
21,600		$^6A_1(S) \rightarrow {}^4T_{2g}(G)$
18,810		$^6A_1(S) \rightarrow {}^4T_{1g}(G)$
17,465	$^6A_1(S) \rightarrow {}^4T_{1g}(G)$	
B (cm^{-1})	642	650
C (cm^{-1})	3552	3594
10*Dq* (cm^{-1})	8811	8948

neutron diffraction data collected at 293 K (with a difference in the unit cell volume by 2.8%; Table 2), which is also reflected by the refined intra-polyhedral bond distances (Table 4). This difference can be ascribed to the different techniques used, if the sample of allactite is considered as chemically homogeneous. However, we cannot exclude a slightly different chemical composition of the crystals used for the X-ray and neutron diffraction experiments, respectively. X-ray and neutron structure refinements lead to a general structure model in agreement with that of Moore (1968), but with much smaller errors for bond distances and location of the H atoms (Table 4). The structure of allactite is built up by sheets of octahedra (two-octahedra wide and held together by vertex-linked octahedra) parallel to (001) (Fig. 1). These sheets are, in turn, held together by chains of linked Mn octahedra and As tetrahedra, running parallel to [010]. The bridging Mn octahedra exhibit corner-, edge- and face-sharing connections (Fig. 1). The four independent Mn octahedra are significantly distorted, but differently, as suggested by the difference between the longest and the shortest Mn–O bond lengths (i.e. Δ_{max}): $\Delta(M1)_{max} \approx 0.13$, $\Delta(M2)_{max} \approx 0.48$, $\Delta(M3)_{max} \approx 0.16$, $\Delta(M4)_{max} \approx 0.20$ Å (neutron refinement based on data collected at 293 K; Table 4). The polyhedron coordinated by As^{5+} is less distorted, with $\Delta(As)_{max} \approx 0.04$ Å. To best quantify relative deviations from the average polyhedral bond length, the bond-length distortion parameters (Δ_{msda}; mean-square relative deviation from the average; Brown and Shannon, 1973) were calculated using the X-ray structure model; $\Delta_{msda}(M1) = 0.0005$, $\Delta_{msda}(M2) = 0.0061$, $\Delta_{msda}(M3) = 0.0006$, $\Delta_{msda}(M4) = 0.0014$ and $\Delta_{msda}(As) = 0.0001$. Consistent with the neutron structure data, the X-ray data show that the most distorted octahedron is *M*2, followed by *M*4 and then by *M*3 and *M*1.

The neutron structure refinements show that four independent H sites occur in the structure of allactite with full site occupancy (i.e. *H*1, *H*3, *H*5 and *H*6; Tables 3*b*,*c*), all as members of hydroxyl groups of the structure (i.e. *O*1–*H*1, *O*3–*H*3, *O*5–*H*5, *O*6–*H*6; Table 4). This is in line with previous studies on raadeite (Chopin *et al.*, 2001) and argandite (Brugger *et al.*, 2011). The principal root-mean-square components of the H-site displacement parameters obtained in this study are fairly anisotropic (as deducible from the data reported in Tables 3*b*,*c*). The O–H bond distances corrected for 'riding motion' effects are listed in Table 4. The complex hydrogen-bonding scheme in the allactite structure is now well defined with at least nine different hydrogen bonds being energetically favourable (Fig. 4, Table 4) with: (i) *O*1 as donor and *O*8 as acceptor (with *H*1···*O*8 = 1.888(3) Å, *O*1···*O*8 = 2.854(3) Å and *O*1–*H*1···*O*8 = 172.0(2)° at 293 K; Fig. 4; Table 4). (ii) *O*3 as donor and *O*5, *O*6 and *O*8 as acceptors, with a tri-furcated configuration (with *H*3···*O*5 = 2.695(3) Å and *O*3–*H*3···*O*5 = 111.2(2)°, *H*3···*O*6 = 2.822(3) Å and *O*3–*H*3···*O*6 = 151.2(2)°, and *H*3···*O*7 = 2.900(3) Å and *O*3–*H*3···*O*7 = 132.1(2)° at 293 K; Fig. 4; Table 4). (iii) *O*5 as donor and *O*3, *O*7 and *O*8 as acceptors, with a tri-furcated configuration (with *H*5···*O*8 = 2.098(3) Å and *O*5–*H*5···*O*8 = 159.9(2)°, *H*5···*O*7 = 2.553(3) Å and *O*5–*H*5···*O*7 = 114.4(2)°, and *H*5···*O*3 = 2.615 (3) Å and *O*5–*H*5···*O*3 = 116.8(2)° at 293 K; Fig. 4; Table 4). (iv) *O*6 as donor and *O*4 and *O*8 as acceptors, with a bi-furcated configuration (with *H*6···*O*8 = 2.197(3) Å and *O*6–*H*6···*O*8 = 154.3(2)°, and *H*6···*O*4 = 2.587(3) Å and *O*6–*H*6···*O*4 = 135.1 (2)° at 293 K; Fig. 4; Table 4).

The strongest H bond of the structure involves *O*1 as donor and *O*8 as acceptor. All the others are comparably weaker (and weak in general), and reflect the bi- or tri-furcated configurations described previously. The described H-bonding scheme is kept at low temperature (Table 4). As expected, the magnitude of the atomic displacement ellipsoids (here described by the expression: $-2\pi^2[(ha^*)^2U^{11} +$

https://doi.org/10.1180/minmag.2016.080.020 Published online by Cambridge University Press

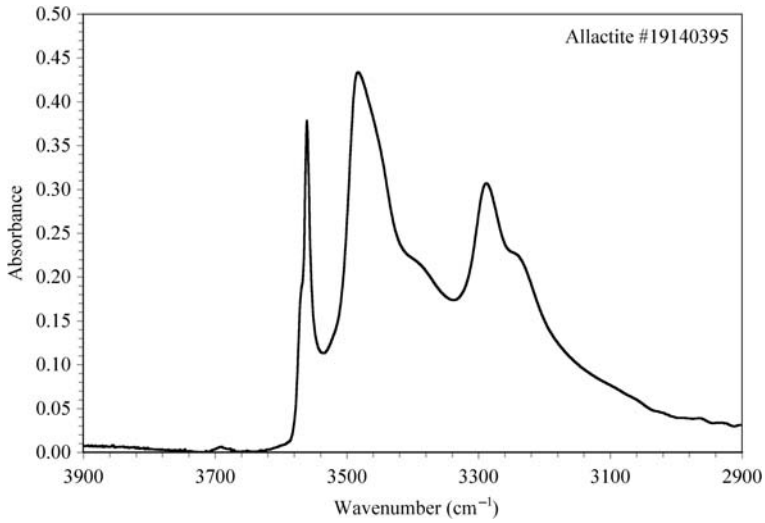

FIG. 3. FTIR spectrum of allactite in the region 3900–2900 cm^{-1}.

$\ldots + 2hka^*b^*U^{12} + \ldots + 2klb^*c^*U^{23}]$) is (on average) reduced by 30% at 100 K, if compared to the values refined at 293 K (Tables 3*b*,*c*). The unambiguous location of all the H sites in the structure of allactite shows that there are two types of octahedral building units in the structure, $^{M1}MO_4(OH)_2$ and $^{M2,M3,M4}MO_2(OH)_4$; no MO_6 unit occurs, consistent with the previous findings for raadeite (Chopin *et al.*, 2001) and argandite (Brugger *et al.*, 2011). The optical absorption experiment of this study confirms that the Mn valence state is 2+, and no evidence of partial substitution, with e.g. Mn^{3+}, is observed.

In the unpolarized FTIR spectrum of allactite (Fig. 3), at least seven OH-stretching bands can be observed distinctly (3236, 3288, 3387, 3446, 3484, 3562 and 3570 cm^{-1}). This suggests that several (OH) environments occur, with different hydrogen-bond strengths. Applying the protocol of Libowitzky (1999), based on observed correlation

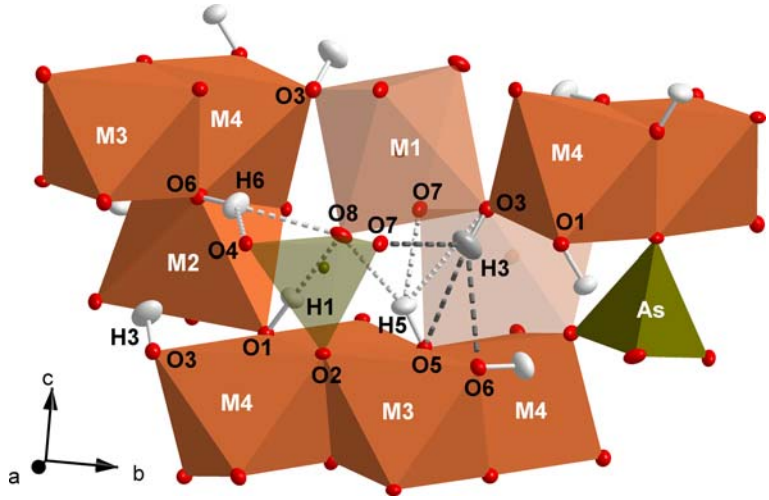

FIG. 4. The H-bonding scheme in allactite, based on the neutron structure refinement of this study (at 293 K). The displacement ellipsoid probability factor is 50%.

https://doi.org/10.1180/minmag.2016.080.020 Published online by Cambridge University Press

between O···H distances and OH-stretching band energies, the recorded OH bands of the present study suggest that O···H distances in allactite range from ~1.81 to ~2.21 Å. Due to a very small slope of the correlation curve for weaker (longer) hydrogen bonds, the indicated upper limit for O···H distances is highly uncertain. For O···H distances in the range of 2.3 to 3.0 Å, the related OH-stretching bands are predicted to occur within a narrow frequency range of merely ~40 cm^{-1}. Infrared spectra of substances with several different hydrogen bonds with O···H distances longer than 2.3 Å, as in allactite, will consequently show considerable overlap, and bands related to different OH environments may not be resolved fully. In addition, it should be pointed out that the correlation curve of Libowitzky (1999) is based mainly on the literature data for O···H distances deduced by X-ray diffraction data, which are known to result in less accurate determinations of H-atom positions. Consequently, the correlation curve may be subject to systematic errors. Taking the aforementioned uncertainties into account, one may conclude that FTIR spectra demonstrate the existence of at least seven different O···H bonds with distances larger than 1.82 Å in allactite. Neutron structure refinements corroborate the FTIR data and their interpretation, with nine independent H bonds and O···H distances ranging between ~1.88 and ~2.90 Å (Table 4). It is interesting to note that the IR of the isostructural minerals raadeite [$Mg_7(PO_4)_2(OH)_8$] and argandite [$Mg_7(PO_4)_2(OH)_8$] show OH-stretching bands in comparable ranges (Chopin *et al.* 2001; Brugger *et al.*, 2011).

Acknowledgements

The authors thank the Institut Laue-Langevin (Grenoble, France), for the allocation of neutron beam time. Chemical analyses were performed with the kind assistance of M. Serracino, to whom the authors express their gratitude. Mark Cooper and an anonymous reviewer are thanked.

References

Brown, I.D. and Shannon, R.D. (1973) Empirical bond-strength-bond-length curves for oxide. *Acta Crystallographica*, **A29**, 266–282.

Brugger, J., Elliott, P., Meisser, N. and Ansermet, S. (2011) Argandite, $Mn_7(VO_4)_2(OH)_8$, the V analogue of allactite from the metamorphosed Mn ores at Pipji, Turtmann Valley, Switzerland. *American Mineralogist*, **96**, 1894–1900.

Bruker (2008) *APEX2, SAINT and SADABS*. Bruker AXS Inc., Madison, Wisconsin, USA.

Burns, R.G. (1993) *Mineralogical Applications of Crystal Field Theory (2nd edition)*. Cambridge University Press, Cambridge, UK.

Busing, W.R. and Levy, H.A. (1964) The effect of thermal motion on the estimation of bond lengths from diffraction measurements. *Acta Crystallographica*, **17**, 142–146.

Chopin, C., Ferraris, G., Prencipe, M., Brunet, F. and Medenbach, O. (2001) Raadeite, $Mg_7(PO_4)_2(OH)_8$: a new dense-packed phosphate from Modum (Norway). *European Journal of Mineralogy*, **13**, 319–327.

Coppens, P., Leiserowitz, L. and Rabinovich, D. (1965) Calculation of absorption corrections for camera and diffractometer data. *Acta Crystallographica*, **18**, 1035–1038.

Dunn, P.J. (1983) Allactite from Franklin and Sterling Hill, New Jersey. *Mineralogical Record*, **14**, 251–252.

Frost, R.L. and Weier, M. (2006) Raman and infrared spectroscopy of the manganese arsenate mineral allactite. *Spectrochimica Acta*, **65A**, 623–627.

Hålenius, U., Bosi, F. and Skogby, H. (2007) Galaxite, $MnAl_2O_4$, a spectroscopic standard for tetrahedrally coordinated Mn^{2+} in oxygen-based mineral structures. *American Mineralogist*, **92**, 1225–1231.

Holtstam, D. and Langhof, J. (editors) (1999) *Långban, the Mines, Their Minerals, History and Explorers.* Raster Förlag, Stockholm.

Howard, J.A.K., Johnson, O., Schultz, A.J. and Stringer, A.M. (1987) Determination of the neutron absorption cross section for hydrogen as a function of wavelength with a pulsed neutron source. *Journal of Applied Crystallography*, **20**, 120–122.

Larson, A.C. (1967) Inclusion of secondary extinction in least-squares calculations. *Acta Crystallographica*, **23**, 664–665.

Lehmann, M. S., Kuhs, W., McIntyre, G.J., Wilkinson, C. and Allibon, J. (1989) On the use of a small two-dimensional position-sensitive detector in neutron diffraction. *Journal of Applied Crystallography*, **22**, 562–568.

Libowitzky, E. (1999) Correlation of O-H stretching frequencies and O-H···O hydrogen bond lengths in minerals. *Monatshefte für Chemie*, **130**, 1047–1059.

Lohr, L.L. and McClure, D.S. (1968) Optical spectra of divalent manganese salts II. The effect of interionic coupling on absorption strength. *Journal of Chemical Physics*, **49**, 3516–3521.

Moore, P.B. (1968) Crystal chemistry of the basic manganese arsenate minerals: II. The crystal structure of allactite. *American Mineralogist*, **53**, 733–741.

Pouchou, J.L. and Pichoir, F. (1984) A new model for quantitative X-ray microanalysis. I. Application to the analysis of homogeneous samples. *La Recherche Aérospatiale*, **3**, 13–36.

https://doi.org/10.1180/minmag.2016.080.020 Published online by Cambridge University Press

Sears, V.F. (1986) Neutron scattering lengths and cross-sections. Pp. 521–550 in: *Neutron Scattering, Methods of Experimental Physics* (K. Sköld and D. L. Price, editors). **23A**. Academic Press, New York.

Sheldrick, G.M. (2008) A short history of *SHELX*. *Acta Crystallographica*, **A64**, 112–122.

Sjögren, A. (1884*a*) Allaktit, ett nytt manganarseniat från Mossgrufvan Å Nordmarksfältet. *Geologiska Föreningens i Stockholm Förhandlingar*, **7**, 109–111.

Sjögren, A. (1884*b*) Kristallografiska studier: VII Allaktit från Nordmarken. *Geologiska Föreningens i Stockholm Förhandlingar*, **7**, 220–236.

Welin, E. (1968) Notes on the mineralogy of Sweden 6. X-ray powder data for minerals from Långban and the related mineral deposits of Central Sweden. *Arkiv för Mineralogi och Geologi*, **4**(30), 499–541.

Wilkinson, C., Khamis, H.W., Stansfield, R.F.D. and McIntyre, G.J. (1988) Integration of single-crystal reflections using area multidetectors. *Journal of Applied Crystallography*, **21**, 471–478.

Wilson, A.J.C. and Prince, E. (1999) *International Tables for Crystallography Vol. C, Mathematical, Physical and Chemical Tables*, second edition. Kluwer, Dordrecht, The Netherlands.

Wright, S.E., Foley, J.A. and Hughes, J.M. (2000) Optimization of site occupancies in minerals using quadratic programming. *American Mineralogist*, **85**, 524–531.

https://doi.org/10.1180/minmag.2016.080.020 Published online by Cambridge University Press